physica status solidi pss a
www.pss-a.com

On-Stage Degradation of Solar Cells Studied Using Capacitance Transient and Luminescence Spectroscopies

Teimuraz Mchedlidze, Katharina Klose, August Weber, Eugen Drubetskoi, Johannes Heitmann, and Matthias Müller*

The light- and temperature-induced degradation (LeTID) of Si-based solar cells remains one of their common stability issues. The degradation process and affecting factors are still widely discussed. Low-temperature photo- and electroluminescence and deep-level transient spectroscopy (DLTS) are rarely used in the LeTID studies. The methods can explore only small-area samples extracted from the cells. A comparison of the fabricated cells in initial, degraded, and regenerated states by these methods is effective only if used for the same location of the cell. The mesa-diodes fabricated from various locations of passivated emitter and rear contact (PERC) PV cells are mounted on the stages of PL/EL and DLTS setups for the initial state characterization. Subsequently, the diodes are subjected to degradation and regeneration treatments under constant bias, and each state is similarly characterized. All processes and tests are carried out on-stage, that is, without moving a diode from the stage. Based on the newly obtained and previously reported results, it is suggested that LeTID reflects hydrogen dynamics between extended defects present in solar cells and hydrogen-containing intrinsic defects formed during/after the contact firing process.

1. Introduction

Since their widespread commercial adoption, Si-based solar cells have faced challenges due to various efficiency degradation mechanisms.[1] The development of a cell-fabrication strategy for low cost and high efficiency gradually overcame many problems with structural defects, metal contamination, and commonly used dopant (boron). Based on the International Roadmap for Photovoltaic,[2] n-type crystalline Si will remain the PV market's dominant base material for the foreseeable future, and the TOPcon cell concept will dominate as PV cell structures.

Light- and elevated temperature-induced degradation (LeTID) of Si solar cells was a later manifested degradation effect.[3–5] LeTID can lead to a decrease of PV conversion e fficiency up to 16% relative and was observed in Si-based n-type and p-type (including Ga-doped) solar cells of various architecture.[6–9] Despite intensive research and unlike other degradation effects, the origin and mechanism of LeTID remain unknown (see refs. [10–14] and references therein).

In recent years, the development of various mitigation techniques for LeTID (see refs. [10,11] and references therein) has downplayed the problem's importance. However, the mitigation treatments increase fabrication costs. Besides that, every update in the cell-fabrication process requires approval for the validity of the previously employed mitigation scheme. Therefore, understanding the LeTID mechanism is still highly desirable.

Only the role of hydrogen in the LeTID effect is probably not questioned now (see refs. [10,14,15] and references therein). Hydrogen is intentionally introduced to the PV solar cells during the last steps of their fabrication, during the contact firing procedure, and sufficiently improves their efficiency.[16,17] Other possible participants in LeTID, like intrinsic defect clusters, structural defects, impurities, dopants, or their complexes, remain under consideration (see refs. [11–13] and references therein). It was found that a B-diffused emitter present during the contact firing procedure is necessary to enable the LeTID effect in n-type Si.[6]

It is also widely accepted that the contact firing step (i.e., a short high-temperature process step at the end of the cell fabrication) is crucial for LeTID occurrence (see, e.g., refs. [18,19] and references therein). Initially, the role of the firing step in the context of LeTID was thought only to provide hydrogen atoms necessary for the phenomenon. However, later research has revealed that the function of the firing step for LeTID is more complex.[20–23]

Spatial heterogeneity of the LeTID process for a single cell was reported for multi-crystalline (mc-Si) cells[5,24,25] quasi-mono-Si[26,27] and for FZ/Cz–Si cells.[25,28] Moreover, as was already noted in ref. [14], the severity of the degradation decreases in order mc-Si → Cz–Si → FZ–Si.[29,30] To some extent, the heterogeneity can be explained by doping irregularities. A clear correlation between degradation level and dopant density, as reported in ref. [27], may be caused by a local increase in the current density for highly doped locations during

T. Mchedlidze, K. Klose, A. Weber, E. Drubetskoi, J. Heitmann, M. Müller
Institute for Applied Physics
Technical University Bergakademie Freiberg
09599 Freiberg, Germany
E-mail: teimuraz.mtchedlidze@physik.tu-freiberg.de

The ORCID identification number(s) for the author(s) of this article can be found under https://doi.org/10.1002/pssa.202500166.

DOI: 10.1002/pssa.202500166

degradation. At the same time, denuded zones around grain boundaries in mc-Si[25] may be formed due to higher resistance and carrier scattering for these locations. Some optical effects related to the photoluminescence from a material containing grain boundaries should also be considered.[31]

Another source of the degradation heterogeneity may be related to structural defects such as dislocations. In the case of quasi-mono-Si cells, we observed a correlation of the degradation severity with the density of structural defects, that is, dislocations.[26,27] Moreover, the deep-level transient spectroscopy (DLTS) signals detected from the degraded sample[27] mostly resembled those detected from dislocations in Si. However, the detected DLTS signals and DLTS trap signatures were not repeated between locations. In ref. [27], we did not measure DLTS in the initial state, and annealing at 200 °C for 20 min was used to recover degraded samples.

DLTS signals from the LeTID-degraded Cz–Si PV modules were recently reported.[28] The signals varied for different locations and were attributed to extended defects. The measured degraded samples were subsequently regenerated by a 3 week short-circuit current at 85 °C. The magnitudes of the signals decreased, and the signatures of the traps changed after regeneration.

Before the present study and following the results presented in ref. [27], we detected DLTS signals from mesa-diodes fabricated at similar locations of sister wafers in initial (Init), degraded (Deg), and regenerated (Reg) states. The detected DLTS signals from three mesa-diodes in each state are presented in **Figure 1**a–c. All detected signals originate from extended defects, as the filling pulse duration dependence measurements proved. Some similarities and successions between the signals can be seen in Figure 1. However, the trap signatures for all detected signals were different, and no clear correlations can be proved.

To exclude the influence of locations on the changes occurring during degradation–regeneration, we decided to study the process for the mesa-diodes prepared from the several locations of the PV cell during on-stage degradation. The initial state and further changes were studied by IV, CV, DLTS, and low-temperature electroluminescence (EL) and photoluminescence (PL) methods.

2. Experimental Section

We used PV cells fabricated in industrial-like PERC technology from B-doped ($N_d \approx 1.1 \times 10^{16}\,cm^{-3}$) Cz-Si crystal, which are prone to boron-oxygen-related LID and LeTID. The initial cell size was M2. The PV cell, in its initial state, was mapped with a PL-scanner at room temperature using laser excitation (Limo180-F400-DL790-EX1359) at 791 nm wavelength and an Andor CCD camera "iKon-M PV-Inspector" for detection. An exposure time was 500 ms. The spatial resolution of the PL map was 170 µm. Two locations with relatively low and high PL signal intensities were selected from the obtained map (see **Figure 2**). The overall PL signal intensity for the L1 location was lower than that for the L2 location. In addition to the top electrical contacts (a busbar and fingers) visible in both images, several elongated vertical dark structures are also visible in the L1 image.

From both L1 and L2 locations, pieces with dimensions $5 \times 10\,mm^2$ (for DLTS) and $10 \times 10\,mm^2$ (for PL + EL) were cleaved. The samples used for spectroscopic studies were attached to pieces of bare Si wafers by asphalt, and the same asphalt was used to cover future mesa-diode areas on the front side of the samples. After hardening of the asphalt, the samples were etched in $H_2O + HF$ (40%) (1:1) solution at room temperature for 3 min to remove the antireflection coating layer (NH_3), rinsed in deionized water, and dried. The rinsing and drying were followed by etching of the samples in solution $5HNO_3(70\%) + 3HF(40\%) + 3CH_3COOH(100\%)$ at room temperature for 2 min with finish in deionized water and drying. After the completion of the procedures, asphalt was dissolved from the samples by subsequent rinsing with benzene, acetone, and propanol. The aforementioned fabrication procedures were selected based on the minimal reverse leakage current from the fabricated mesa-diodes.

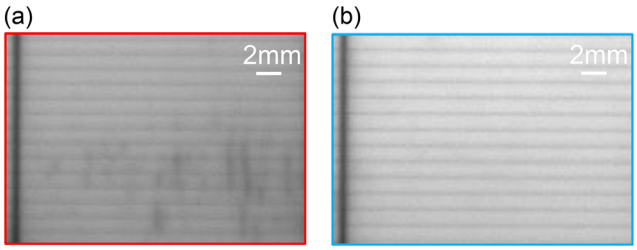

Figure 2. Images obtained by the PL scanner for locations a) L1 and b) L2 of the PV cell in the initial state.

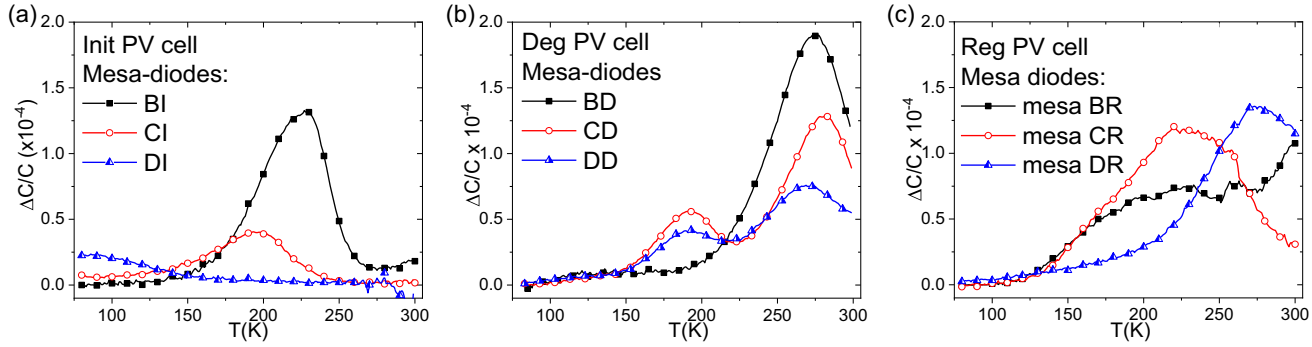

Figure 1. DLTS spectra detected in three "sister" locations of solar cells in a) Init, b) Deg, and c) Reg states. Measurement conditions: $V_R = 5$ V, $V_P = 0.5$ V, $t_P = 1$ ms, $t_D = 75$us, signal rate (SR) and maximum bandwidth (MBW) 54 kHz, number of transitions averaged $N_{trans} = 200$. The spectra are presented for rate window $RW = 60\,s^{-1}$.

The areas of the mesa-diodes used in the DLTS study ranged from 2 to 4 mm^2, and those used in PL were 30–60 mm^2. The remaining parts of the fingers and the back contact of the cell were used for electrical contacts to the mesa-diodes. Sample images of the fabricated and mounted mesas on the measurement stages can be found in ref. [32] (see slide 6).

Current-induced degradation (CID) at elevated temperatures is frequently used to model LeTID.[10] However, due to leakage current at the perimeter of mesa-diodes, especially for small-area mesa-diodes used for DLTS studies, it is preferable to use constant voltage-induced degradation (CVID). We confirmed the equivalence of the CVID and CID degradation/regeneration processes by IV and CV measurements for the large-area samples. In the case of CVID, the current through the pn-junction corresponds to the applied forward voltage and is not affected by the perimeter leakage. The parameters of the CVID at a relatively large-area sample (1 cm^2) were used for the degradation–regeneration procedure of small-area mesa-diodes. The degradation–regeneration curve for the large sample cut-out from the L1 location is presented in **Figure 3**.

The maximal LeTID effect for the sample was achieved after the $t_{deg} = 55$ mins at the stage temperature $T_P = 369$ K under a forward bias of 470 mV. After an additional $t_{reg} \approx 6$ h under the same conditions, the sample was mostly regenerated (see Figure 3). The obtained T_P, V_F, t_{deg}, and $_{Treg}$ parameters for CVID were later applied for the degradation/regeneration of mesa-diodes used in DLTS and PL-EL studies.

During the study, we measured IV and CV dependencies for each mesa-diode in each Init, Deg, and Reg state. These measurements were done using a Keysight B1500 characterization unit in the range $V_R = 5$–0 V and 20–50 mV bias steps at 300 K.

A DLTS setup used in the study was built on the base of MFIA, a dual-phase digital lock-in amplifier, and an LCR meter from Zurich Instruments (see refs. [32–34] for more details). Such a setup showed enhanced sensitivity to the extended defects in previous studies.[34] Biasing and pulsing sequences during the DLTS measurements were performed using a Keysight 33500B pulse generator. The scheme and more details about the setup can be found in ref. [32] (see slide 27).

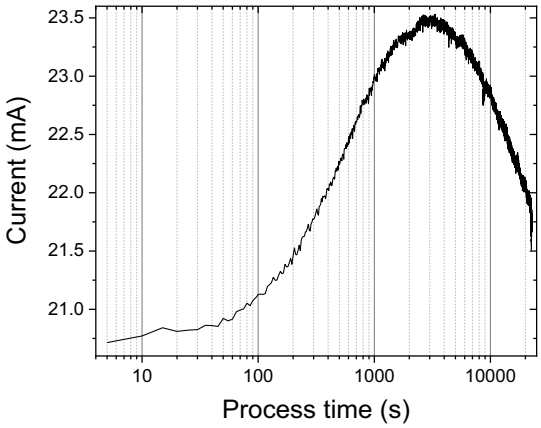

Figure 3. Degradation-regeneration CVID process curve for 1 cm^2 area PV cell cleaved from the L1 location. The process parameters: $T_P = 369$ K, V_F(const) = 470 mV, dark conditions.

The low-temperature PL and EL (LT-PL-EL) were measured using a He closed-cycle cryostat from Cold Edge, equipped with Sumitomo RDK-408 cold head. The PL-EL spectra were detected at $T_{meas} = 10$ K. We used a similar detection scheme (lock-in + PMT) for electro (EL) and light (PL) excitation. PL was excited with a CW laser/chopper scheme (at 532 nm wavelength). For EL, we used a Keysight 33500B pulse generator applying forward 5 V or reverse 11 V pulses with $t_p = 6$ ms duration during a 12 ms total sequence. More details about the PL-EL setup can be found in ref. [32] (see slide 26).

3. Results and Discussion

3.1. Static Electrical Measurements

The exact active area of the fabricated mesa-diodes is difficult to determine with necessary precision. Estimations based on the image will not be precise since the surface of the cells is structured for enhanced light absorption.[35] Estimations from CV measurements and the average base doping level of the PV cell material can also be faulty since the local doping level and doping profile after emitter formation may vary. Therefore, comparing leakage current or doping densities for various mesa-diodes in various degradation states cannot be accurate enough. Example IV and CV curves for one of the mesa-diodes in Init, Deg, and Reg states from the L1 location of the solar cell are presented in **Figure 4**.

Since all static measurements were done using the same biasing sequence at the same temperature, the relative changes caused by degradation/regeneration in IV and CV curves for each mesa-diode can be recognized as sufficiently accurate. Therefore, for each value of applied bias, ratios of leakage current (I_{leak}(Deg)/I_{leak}(Init) and I_{leak}(Reg)/I_{leak}(Init)) and dopant density (N_d(Deg)/N_d(Init) and N_d(Reg)/N_d(Init)) were calculated from IV and CV measurement data. After that, the average and standard deviation over the investigated voltage ranges were calculated for each set of the ratios. The results are presented in **Figure 5**a,b.

Leakage current ratios show an overwhelming influence of changes (decrease) for the mesa-diode perimeter leakage (see Figure 5a). The leakage current was strongly suppressed by degradation treatment at 369 K, and further decrease continued during the regeneration treatment. Such tendency was characteristic for all mesa-diodes measured; however, the quantitative characteristics of the effect varied. We cannot speculate if this was only a temperature effect or if the current through the perimeter also played a role. However, these observations again illustrate why the CVID procedure instead of the CID should be used for degradation/regeneration treatments of mesa-diodes. Moreover, the substantial decrease of the perimeter leakage current during the treatments excludes the possibility of degradation monitoring for small diameter mesa-diodes since a significant part of the changes will be conditioned by anneal-out of perimeter leakage paths.

Unlike the leakage current, changes in the doping level for the L1 location significantly differ from that for L2. For the L1 location, N_d decreases during the degradation and partly restores during the regeneration. The decrease of N_d during degradation is significantly smaller for the L2 location, and the decrease

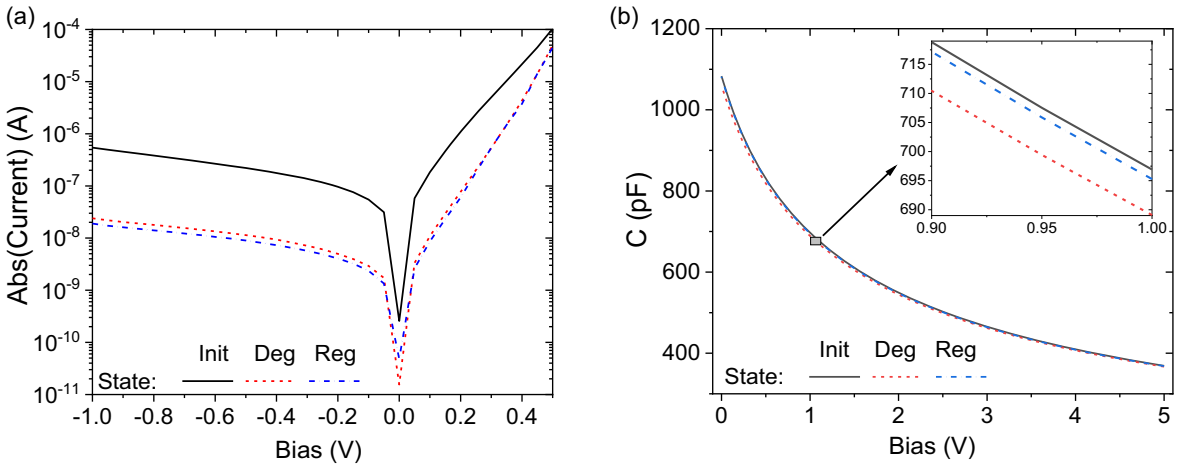

Figure 4. a) IV and b) CV dependences for Init, Deg, and Reg states of one of the mesa-diodes from L1 location at $T_{meas} = 300$ K. The insert in (b) shows details near 1 V bias value.

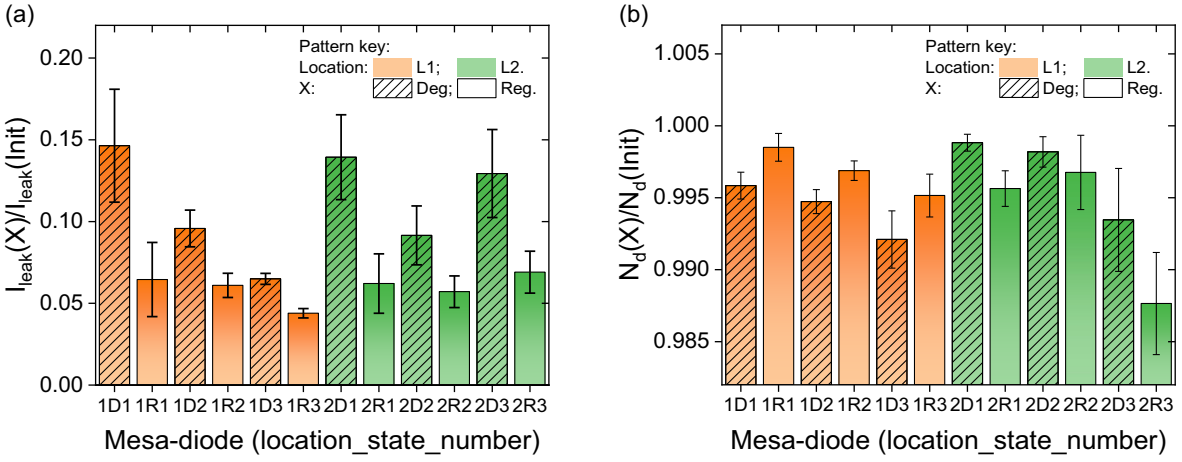

Figure 5. a) Ratios of leakage currents and b) dopant densities in degraded and regenerated states to that in the initial state for L1 and L2 locations of the solar cell. In each case, three mesa-diodes (1D1-1D3 and 2D1-2D3) were measured.

continues during the regeneration treatment. Despite the small differences and nearly overlapping error bars, these observations support the degradation mechanism, which will be discussed later.

3.2. DLTS Measurements

Proper DLTS signals from the majority-carrier traps were detected for all measured mesa-diodes fabricated from the L1 location of the PV cell in the Init state. The signals with changed trap signatures and intensity were also detected after degradation and regeneration procedures. Detected DLTS spectra from three mesa-diodes (B, C, and D) in Init, Deg, and Reg states for the rate window RW = 10 Hz are presented in **Figure 6**.

The signatures of the detected traps obtained after the standard DLTS data treatment procedure (from the Arrhenius plots) substantially scatter. Signatures of traps previously reported in DLTS investigations of LeTID (to the best of our knowledge[27,28,36–38]) correspond well to those of the signals detected in the present work. For the measured mesa-diodes, the thermal excitation energies and pre-exponential factors suggest an increase in the recombination activity of the traps in the degraded state and a decrease in the activity after regeneration. From **Figure 7**, where averaged values of the trap parameters are presented, the increase of activation energy and pre-exponential factor for the degraded state can be well seen.

The trap signature parameters obtained from the DLTS measurements usually do not correspond directly to the energy level positions and carrier capture cross-sections of the trap (see, e.g., refs. [39,40] and references therein). The above is especially true for the case of extended defects like interfaces, dislocations, precipitates, and the like.[41] The traps detected in our study belong to localized states of extended defects, similar to those reported in refs. [27,28] The extended nature of the defects was confirmed for all detected signals by measuring DLTS peak intensity dependence on the trap-filling pulse duration. An example of the

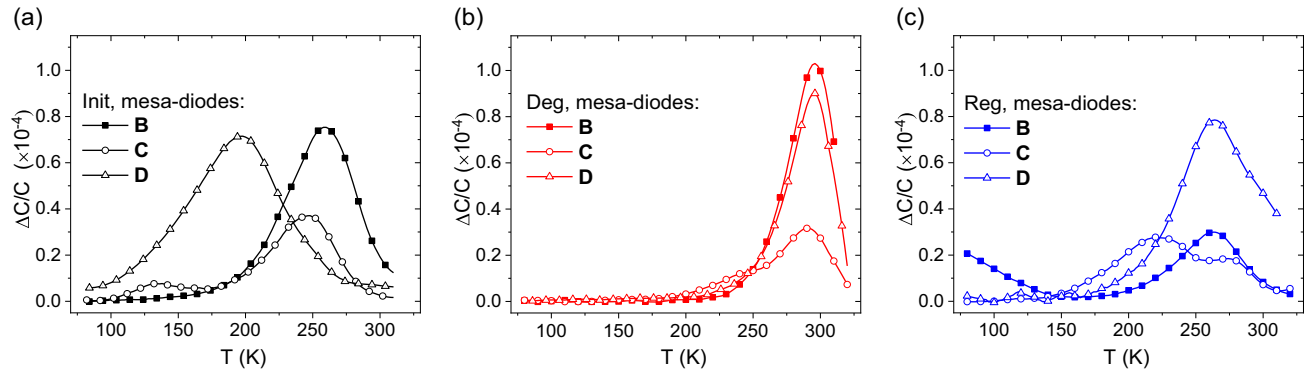

Figure 6. DLTS spectra detected from three mesa-diodes (B, C, and D) fabricated from the cell in the L1 location in a) initial, b) degraded, and c) regenerated states. The noise in the spectra was smoothed. See the spectra below for the actual noise level (Figure 9).

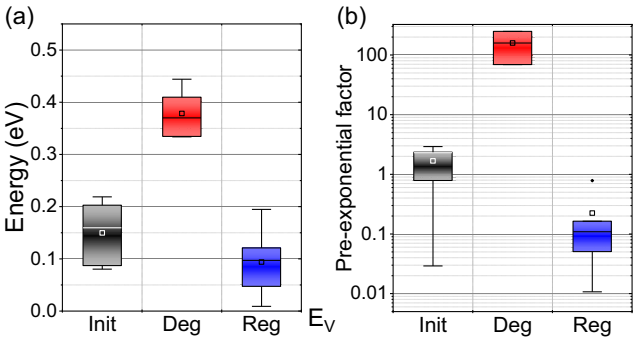

Figure 7. a) Averaged values for the trap E_t and b) pre-exponential factors obtained from the analysis of DLTS data from Init, Deg, and Reg states of mesa-diodes cut-out from the cell in the L1 location.

dependence of the detected DLTS spectra on the filling pulse duration is presented in **Figure 8**.

The exact nature of the extended defects responsible for the detected DLTS peaks can be only speculated. The signatures of the detected traps in the present study and those reported earlier[27,28] well correspond to those related to dislocations in

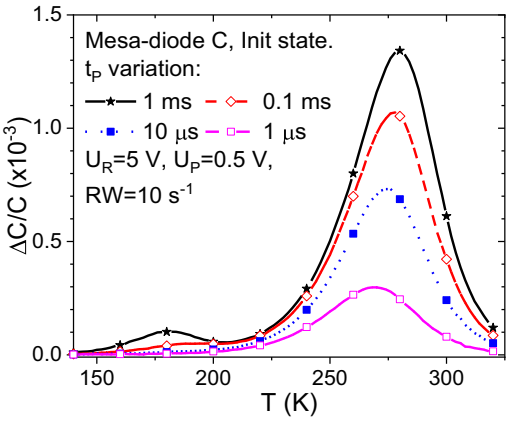

Figure 8. Variations of the detected DLTS spectra with the filling pulse duration for the mesa-diode C from location 1 (see Figure 6). Measurement parameters are presented in the figure.

Si (see, e.g. refs. [41–43], and references therein). The presence and influence of dislocations in crystalline Si used in the PV industry were recently underlined.[44,45] Other aspects and details of possible participation of dislocations in LeTID will be discussed later.

Enhanced sensitivity of the DLTS setup[34] was especially in high demand during registering DLTS signals from mesa-diodes fabricated from the L2 location of the solar cell. Example spectra detected from the mesa-diodes fabricated from the material of L1 and L2 locations are presented in **Figure 9**. The high-contrast lines in the figure represent smoothed signals, and low-contrast images show the original data. Repetitive measurements for several mesa-diodes confirmed the validity of the smoothing procedure used and excluded the influence of random noise. On average, the DLTS signal strength detected from L2-located mesa-diodes was at 0.1 level compared to those from L1.

All signals detected from the L2 location can also be attributed to extended defects. We checked signal dependence on the filling pulse duration for several mesa-diodes, and in all cases, the change from 1 ms to 10 μs in t_p duration suppressed the signal level twice and more. For L2-located mesa-diodes, it was not possible to reliably obtain trap signatures from the DLTS spectra due to small signal/noise ratios. However, the shape of the peaks and their positions suggest their relation to similar defects as in the case of L1 but in significantly smaller densities. It is worth noticing that using a standard DLTS system, the signals detected for the L2 location would mostly remain under detection limits.

3.3. Luminescence Measurements

We studied low-temperature ($T_{MEAS} = 10$ K) luminescence from the on-stage LeTID processed mesa-structures in three different regimes: photoluminescence (PL), electroluminescence under forward (ELF) bias, and under reverse (ELR) bias (see **Figure 10**). To our knowledge, low-temperature ELF and ELR were not used previously in solar cell studies. Therefore, we compared the detected EL spectra to those from low-temperature PL (LT-PL). While PL, excited under 532 nm laser illumination, represents radiative recombination processes (RRP) in near-junction volume,[46–48] ELR represents RRP from volume located deeper inside the cell base.[45] The observed ELF spectra resemble RRP,

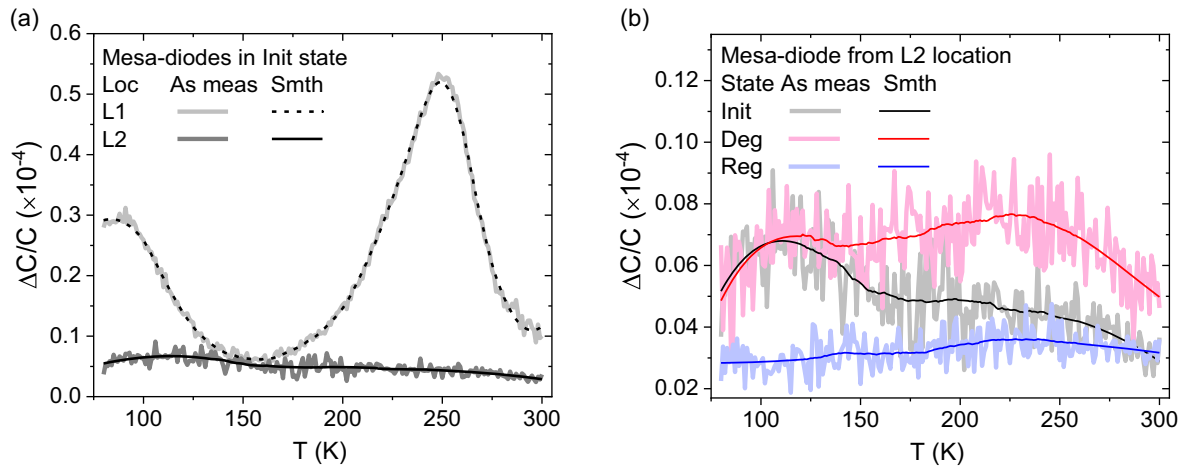

Figure 9. a) Example spectra detected from mesa-diodes prepared from the PV cell material from L1 and L2 locations in the Init state and b) an example DLTS spectra detected from the mesa-diode from the L2 location in three Init, Deg, and Reg states. Measurement conditions: $U_R = 5$ V, $U_P = 0.5$ V, and $t_P = 1$ ms, spectra are presented for the rate window RW = 100 s^{-1}. Low contrast lines present original data, while high contrast lines represent the smoothed curves.

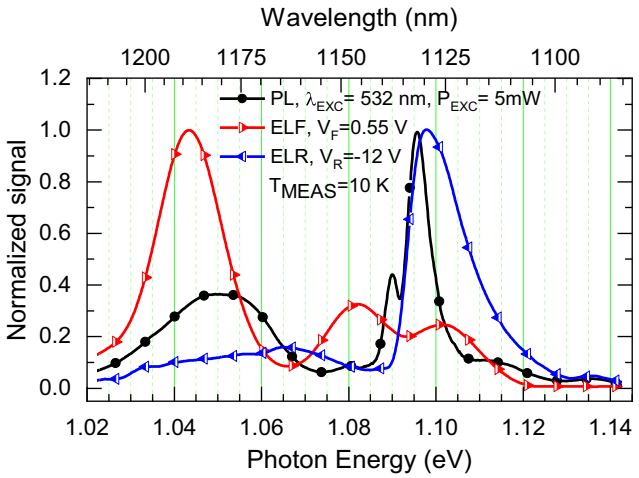

Figure 10. PL, ERF, and ELR spectra detected from the Reg state of a mesa-diode fabricated from the L1 location. The measurement parameters and curve attributions are indicated in the figure.

which is usually detected from p-type Si heavily co-doped with Phosphorus, for example, from the emitter volume.[46,49,50] Besides comparing the obtained PL, ELF, and ELR spectral shapes to those reported previously for LT-PL, we carried out TCAD modeling for the distribution of radiative recombination rates using parameters of the studied solar cell. The simulation results fully confirmed attributions of the EL spectra to different depths in the cell (for more details, see ref. [32]).

Our attempts to detect radiative recombination of carriers from dislocations in both L1 and L2 locations failed. The reason may be insufficient sensitivity of our PL setup and/or non-radiative character of recombination for the dislocations. Therefore, we concentrated on the luminescence signals in the 1.02–1.14 eV photon energy range corresponding to near bandgap luminescence. The three PL, ELF, and ELR spectra from L1 located mesa-diode in Reg state are presented in Figure 10. The spectra are normalized on their maximal intensity. Except for minor (within the measurement error) variations in the luminescence intensity, we did not detect any changes for different states of the LeTID for the L2 location.

Indicative changes were noticed during the on-stage degradation of the mesa-diode fabricated from the L1 location. The ELR spectra reflected overall degradation/regeneration kinetics. The intensity of the ELR spectra decreased after Deg treatment and was almost restored in the Reg state (not shown). The changes observed for the PL and ELF spectra were more informative. These changes are presented in **Figure 11**a,b. The luminescence intensity for ELF spectra was normalized on the fitted intensity of the IB^{NP} line (non-phonon recombination process for impurity band[49]). In the case of PL spectra, the intensity was normalized on the fitted intensity of the I^{NP}(FE) line (non-phonon recombination of free exciton[51]). These normalizations were necessary to exclude the influence of possible variations in the setup during LeTID procedures. Consequently, all changes in the spectra are relative to the peaks used for the normalization.

For both PL and ELF, the spectra are similar in the case of the Init and Reg states of the cell. Substantial changes for Deg state can be noticed in PL spectra in the HDBB + DA range (1.02–1.06 eV)[46,49] and for I_{BTO}(BE), I_{TO}(FE) peaks (1.09–1.10 eV).[51] For the ELF spectra, changes are seen for P-B_{TO} (1.04 eV), DA range (1.04–1.07 eV), and P-B_{TA} (1.08 eV). All these changes can be explained by decreased active boron concentration in the emitter and near-emitter volumes. Indeed, according to the models of radiative recombination in heavily phosphorus-doped Si,[49,51,52] the changes observed in PL and ELF spectra in the 1.02–1.08 eV range can be related to the deficit of active boron in the volume responsible for the luminescence, that is, in the emitter volume, causing suppression of donor-acceptor recombination processes. A similar decrease in active boron concentration in nearby emitter volume can be responsible for the observed changes with boron-related

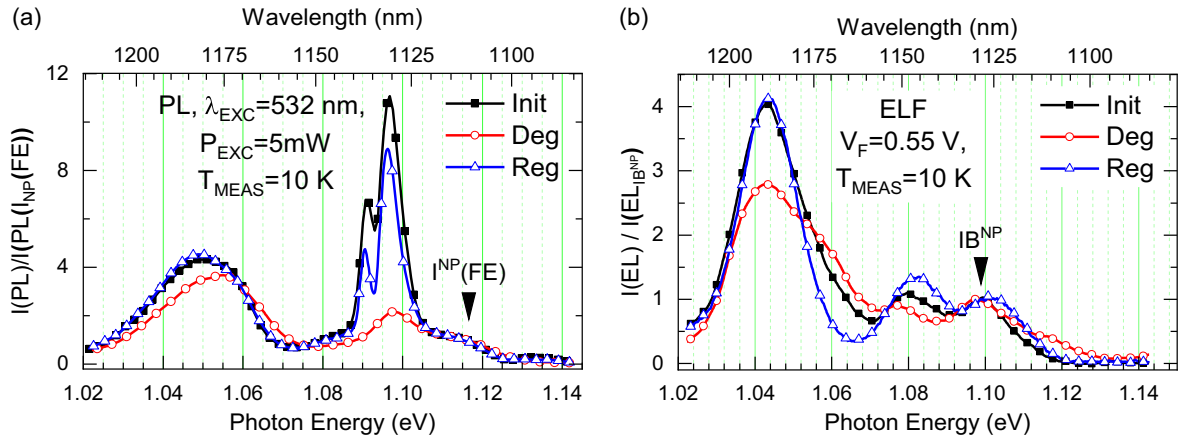

Figure 11. a) PL and b) ELF spectra detected from the L1-located mesa-diode. The spectra were detected in the Init, Deg, and Reg states, as indicated in the figure. Intensities are normalized to fitted intensities of the I^{NP}(FE) line (at 1.16 eV) in the case of (a) and on the IB^{NP} line (at 1.098 eV) in the case of (b). Arrows in the figure indicate the positions of these lines.

excitons in PL spectra (1.09–1.1 eV). Therefore, the observations suggest decreased active boron concentration in the Deg state. The total amount of the active boron deficit in the Deg state may not be so significant according to the models.[50,52]

3.4. Discussion

The possible interaction of boron with hydrogen during degradation was recently broadly discussed (see ref. [13] and references therein). Our static electrical and luminescence studies showed partial deactivation of boron, probably by the formation of acceptor–hydrogen pairs in the degraded state for the L1 location. Interestingly, in the location with less density of extended defects, namely L2, this effect was less pronounced and, moreover, was not reverted during regeneration. The observed deactivation of boron can also contribute to a decrease in cell efficiency. However, considering the small concentration changes, the effect can be considered minor.

Change in the DLTS spectra during LeTID treatment was the pronounced effect observed in this study. The possible source of such changes can be an interaction of hydrogen atoms with the extended defects.[53] The interaction of various defects and dopants with hydrogen in Si has been a widely discussed topic for a long time (see e.g., refs. [13,54,55] and references therein). The suppression of the electrical activity of dislocations in Si by hydrogen[53,56,57] and the possible competition of this process with dopant passivation[57] were also broadly discussed. From the obtained DLTS results, we can suggest that dislocations partly lose hydrogen during the degradation step. The loss of hydrogen enhances dislocation-related carrier recombination processes and suppresses PV cell efficiency. During the regeneration, hydrogen passivates the dislocations again, causing suppression of their recombination activity, and PV cell efficiency is restored.

The difference in the DLTS spectra in the initial and regenerated states from each other can be explained by variations of possible configurations in the dislocation-hydrogen system.[17,58] From the theoretical calculations, it was suggested that hydrogen has enhanced mobility along the dislocation core in comparison to the Si bulk, and it can substantially change the dislocation core structure during interaction.[53,55,59] Hydrogen atoms are usually trapped at kinks[59] or antiphase defects[60] along the dislocation core. It was estimated that hydrogen density at the dislocation core can be as high as six atoms per Burgers vector, depending on the type of the dislocation.[59] This number renders dislocations as a massive reservoir of hydrogen in silicon bulk after hydrogen enters the bulk due to the firing step.

The dislocations passivated by hydrogen and losing it during degradation well suit the observed inhomogeneity of LeTID:[26,27] the effect correlates with their density. Moreover, in agreement with the supposition about the crucial role of dislocations in LeTID, for the sequence of mc-Si → Cz–Si → Fz–Si, the severity of LeTID falls in parallel with the density of extended defects in these materials.[14,61]

The reason why hydrogen leaves dislocations during degradation and later returns during regeneration needs to be found. One possibility is that a strong sink for hydrogen activates in the wafer bulk near dislocations during degradation and later disappears during regeneration, releasing hydrogen back. The sink is likely to be formed during the contact firing step;[18,19] let us denote it as a firing-induced defect (FID). The proposed LeTID scheme is presented in **Figure 12**. We will discuss the electrical activity of FID at various degradation stages later. However, even if we assume zero electrical activity for FID at all stages, the proposed LeTID scheme will work due to changes in the recombination activity of the extended defects (i.e., dislocations).

Before trying to understand the origin of FID in the bulk of the cell, let us consider the possible defect formation inside the emitter during the firing procedure. Considering the composition of the P-doped emitter (high phosphorus concentration in Si) and the conditions of the firing procedure (800–850°C, RTA), we can expect the formation of small phosphorus-silicide precipitates there. Indeed, the steady-state nucleation rate for the SiP precipitates in Cz–Si has a maximum of around 800 °C.[62] The reported critical P concentration for the precipitate formation is 3×10^{19} cm^{-3},[62] which is even below the expected phosphorus concentrations in solar cell emitter.[63] Moreover, RTA conditions

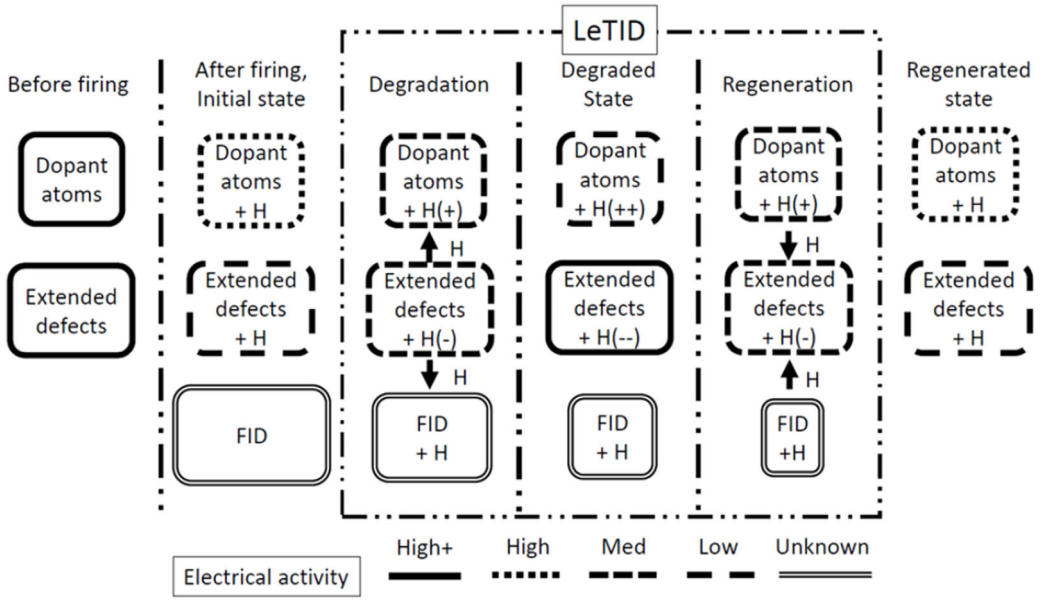

Figure 12. Proposed scheme of the LeTID effect. Each stage is shown as a labeled column. The electrical activity (activated dopant concentration and recombination activity of extended defects) is depicted using differently punctuated lines (see the legend below). The shrinking area of the FID indicates the change in defect density. The arrows show supposed hydrogen dynamics. A part of hydrogen atoms (not shown in the sketch) also goes to the emitter and surfaces of the cell (see, e.g., ref. [15]).

(non-equilibrium generation of interstitials and vacancies at the firing temperature) also support the formation of SiP precipitates at these temperatures. All this suggests that the formation of SiP precipitates due to the firing procedure is probable. It was also observed that the precipitates induce strain in the lattice.[62] These precipitates hardly affect the efficiency of the cell but can interact with hydrogen atoms during LeTID. In our study, we noticed substantial changes in the spectra of degraded samples during ELF and PL experiments. These changes may be related to hydrogen inflow to the emitter during LeTID and its reactions with dopants and SiP precipitates. Besides that, the formation of SiP precipitates suggests that the P-doped emitter will not inject interstitials into the Si bulk during firing.

Interestingly, for observations of LeTID in P-doped Si, the presence of a B-doped emitter during the firing step was critical.[6] Without a B-diffused emitter, n-type samples showed only degradation related to the sample surface. On the contrary, the presence of a P-diffused emitter atop the P-doped base during the firing procedure showed a slight improvement in carrier lifetime in LeTID conditions.[6] Both B and P atoms diffuse in Si under the mediation of silicon interstitials (^{Si}I); however, the activation energy for P diffusion is substantially smaller.[64] This is attributed to the stronger binding of the P^{Si}I complex in comparison to B^{Si}I and suggests that the inflow of interstitials to the base during the firing procedure will be higher in the case of a B-doped emitter. The possible formation of SiP precipitates in a P-doped emitter[62] will further increase the difference between the effect of P- and B-doped emitters. Silicon interstitials, ^{Si}I formed in B-doped emitter will move fast into the base due to their higher mobility (see refs. [64,65], and references therein). Therefore, we can suppose that the difference in LeTID behavior for the P-doped base between the P-doped and B-doped emitter should be related to interstitials injected into the base during the firing step.

The aforementioned supposition can be supported by the reported influence of nitrogen doping level on LeTID severity in p-type FZ-Si.[38] Indeed, the authors report that the extent of degradation in the nitrogen-rich samples is at least double that of the nitrogen-lean samples. Nitrogen doping (i.e., crystal growth in a nitrogen atmosphere) is used to suppress the formation of vacancy-related defects (COPs, and alike) in the Si crystal after growth (see refs. [66,67] and references therein). Therefore, the nitrogen-rich crystal contains fewer vacancies for annihilation with ^{Si}I during the firing step. Besides that, in the recent report, it was also recommended to increase the number of vacancy-related using modification of the crystal growth procedures to mitigate the LeTID effect.[68] The other group of authors reports that the LeTID effect in Cz-Si-based cells is strongly enhanced whenever oxygen precipitation occurs in the cell-fabrication process.[69] Since the formation of oxide precipitates is known to inject interstitials to the Si bulk (see, e.g. refs. [70,71], and references therein), these results also indicate that Si interstitials enhance LeTID.

In most experiments on LeTID in p-type Si, the firing was done without an emitter (see ref. [72] and references therein). Therefore, the influence of possible defect formation in the emitter during the firing process on the LeTID can be ignored for p-type Si. The stronger binding of ^{Si}I to P compared to B[64] may suggest the elevated presence of interstitials in B-doped base material compared to that of P-doped. The simultaneous strong hydrogen inflow and presence of ^{Si}I spaces during the firing step will lead to their interaction at the peak temperature and during cooling. Possible reactions were thoughtfully investigated (see refs. [65,73–76] and references therein). The temperature range

and the lowest formation energy[77] favor bonding of self-interstitial to two hydrogen atoms ($^{Si}IH_2$). At the same time, due to high temperatures and a high inflow of hydrogen atoms, the vacancies that emerge will most probably form VH_4 defects.[78,79]

The existence and structure of the $^{Si}IH_2$ and VH_4 defect were reported after careful investigation of infrared absorption spectra (FT-IR spectroscopy) of the proton-implanted and electron-irradiated silicon samples (see refs. [80,81] and references therein). To the best of our knowledge, the defects do not show any electrical or paramagnetic activity[65] and are stable up to 500°–650°C (see ref. [81] and references therein). The formation of other ^{Si}I-hydrogen and V-hydrogen complexes due to the firing procedure cannot be excluded but is less favorable. Besides that, almost all other complexes are electrically active and/or anneal out at much lower temperatures.[65,82] The electrical inactivity of $^{Si}IH_2$ and VH_4 well suits the fact that they were not detected in the samples after the firing procedure. To the best of our knowledge, FT-IR detection of $^{Si}IH_2$ or VH_4 complexes in LeTID-related samples has not yet been attempted.[68,83–85]

A study of a possible influence of VH_n ($n = 1,...,4$) defects on LeTID was performed using electron-irradiated p-type Si.[86] In the study, Si was irradiated with low energy (1 MeV) electrons to various doses before or after the firing procedure. No LeTID effect was observed if the firing procedure preceded the irradiation; however, the lifetime strongly decreased with the irradiation dose. For the reversed sequence (i.e., when irradiation preceded the firing procedure), the LeTID effect proceeded in the usual way, suggesting that the presence of radiation damage before firing had no impact on the post-firing LeTID.[86] The authors conclude that variation in the concentration of vacancy clusters in the wafer bulk does not influence LeTID.

Therefore, we suggest that the $^{Si}IH_2$ defect be considered a possible FID candidate. In this supposition and according to the proposed LeTID mechanism, hydrogen in the wafer bulk is contained in dopant-hydrogen pairs and $^{Si}IH_2$ and VH_4 defects after the firing step. Besides that, the most significant amount of hydrogen is trapped at/inside the structural defects, i.e., dislocations. At the LeTID conditions, part of hydrogen from the dislocations is dissolved to the surrounding volume and interacts with $^{Si}IH_2$ defects by the scheme like

$$\begin{aligned}\{^{Si}IH_2\} &\rightarrow \{^{Si}IH_2\}* + H \rightarrow \{^{Si}IH_3\}* \\ &\rightarrow \{^{Si}IH\}* + H_2 \rightarrow {}^{Si}I + H + H_2\end{aligned} \quad (1)$$

As a result, silicon self-interstitial moves to the sample surface or nearby dislocations and recombines there. The possible scheme (1) of transformation/dissolution for $^{Si}IH_2$ is not unique. A computer simulation should be performed to find the most favorable scheme. The released hydrogen interacts with dislocations and dopants and moves to the sample surfaces. When all $^{Si}IH_2$ defects in the volume near the dislocation dissolve, the LeTID process for the location is finished, and the volume is regenerated. Recombination activity in the degraded state is mainly related to the traps at the non-passivated dislocations that lost hydrogen; however, the intermediate products of the reaction (as shown in (1) or similar) may also contribute.

The proposed mechanism well explains the results of experiments with dark annealing (DA) and repeated light soaking (LS) cycles.[87,88] The degradation severity after each (LS + DA) circle decreases since the density of $^{Si}IH_2$ defects near dislocations falls due to their dissolution. The regeneration during DA treatment is probably due to hydrogen atoms returning to dislocations at the specific DA temperature[89] but without carrier injection. It is interesting to note that after each (LS + DA) cycle, the effective carrier lifetime was slightly improved (for 4 μs after nine cycles.[87] This improvement may indicate changes in the dislocation structure caused by multiple interactions with hydrogen atoms and/or interstitials resulting from $^{Si}IH_2$ dissolution. Besides interaction with dislocations, the hydrogen atoms freed after the $^{Si}IH_2$ dissolution may also be involved in the dopant passivation, in the reactions in the emitter observed in this study and reach the cell surface.[15]

It should be noted that VH_4 defects formed at/after the firing procedure in the proposed scheme remain inactive at all stages of the LeTID process. Their migration and interaction with $^{Si}IH_2$ defects or hydrogen atoms is unlikely under LeTID conditions.[78]

A recent publication[90] reported the electron spin resonance (ESR) study of the LeTID process. The authors observed substantial growth of an isotropic ESR peak with a *g*-factor of 2.006 for the degraded state and its decrease for the regenerated state. The peak was identified as originating from Si-broken bonds. The ESR peak with similar parameters was previously observed in Si with dislocations (so-called Si-Y ESR line, see refs. [91,92] and references therein) and attributed to "dislocation dangling bonds". Unfortunately, the authors in ref. [90] present only room temperature measurements for a single orientation. Therefore, the possible structure of the dislocation-related peak(s) cannot be observed and analyzed. The appearance of a hydrogen-related double-peak in the presented spectra[90] may be attributed to either hydrogen bonded to dislocation or to one of the modifications occurring with the $^{Si}IH_2$ defect (see Equation (1)). Further ESR study will be helpful for the understanding of the exact LeTID mechanism.

The presence of impurities proved not to be critically important for the LeTID process,[10] which also well suits the proposed mechanism. However, the influence of the impurities on the LeTID effect can be significant. Namely, metal impurities can influence (enhance) the electrical activity of dislocations in a non-passivated (degraded) state.[93] Carbon, nitrogen, oxygen, iron, and some other impurities influence the vacancy/interstitial balance in the Si crystal and, therefore, can enhance or suppress the formation of $^{Si}IH_2$ defects.[69,94–96] Similar effects can be related to the dopant type and concentration. If the proposed mechanism for LeTID degradation is proved, the growth of vacancy-rich FZ- and Cz-Si crystals[95] for PV applications can be considered advantageous.

Further studies will be necessary to confirm the existence of the proposed LeTID mechanism. Detecting the $^{Si}IH_2$ characteristic signal using the FT-IR technique in the p-type Si after the firing procedure will be crucial. The FT-IR frequencies for the $^{Si}IH_2$ defect are well documented.[80] However, one should carefully consider the detection limits of the FT-IR setup at the measurement temperature. Preferably, low-temperature ($T_{MEAS} \leq 77$ K) measurements with high resolution near

$1880\,cm^{-1}$ wavenumber should be performed on Si material before and after contact firing and at different stages of LeTID. If the proposed mechanism is correct, the decrease in the density of $^{Si}IH_2$ defects after regeneration should correlate to the severity of degradation. Also, it will be interesting to study LeTID for samples where a highly B-doped layer will be present on B-doped base silicon during the firing step. Such a structure will increase the inflow of Si self-interstitials to the base and increase the severity of the LeTID effect compared to the P-doped emitter.

4. Summary

Applying electrical and luminescence methods to study the LeTID process in solar cells with PERC structure "on-stage" revealed new and significant information about degradation. For the first time, local degradation was studied on-stage, that is, all local electrical and optical investigations were done during the LeTID process (degradation–regeneration) using the cell material from the same location without moving it from the measurement stage. To our knowledge, low-temperature electroluminescence under forward and reverse bias was not employed previously for solar cell degradation studies and can give valuable information about degradation-related changes in the emitter and bulk of the cells.

The results of this study and information from previous publications allowed us to propose a mechanism for the LeTID process that consistently explains the known facts associated with the effect. The efficiency decrease in the LeTID process was proposed to occur due to the enhancement in the recombination activity of extended defects (dislocations) in the bulk of the cells. The enhancement is related to releasing passivating hydrogen atoms from the dislocations. Under LeTID treatment conditions, hydrogen atoms are attracted by $^{Si}IH_2$ complexes formed in the volume of the cell due to the contact-firing process. Hydrogen causes stress relief around the defects and their transformation/dissolution. After $^{Si}IH_2$ dissolution, the released hydrogen neutralizes the electrical activity of dislocations, bringing the cell to an efficiency state close to the initial one. Additional impurities, dopants, and fabrication processes can enhance/suppress the intensity and accelerate/retard LeTID by affecting the recombination strength of dislocations or changing the conditions for $^{Si}IH_2$ formation. We do not exclude the possibility that other degradation mechanisms can act in parallel to the proposed one.

Although the presented results and conclusions are primarily relevant to Si solar cells and related technologies, similar defect interaction mechanisms in silicon may be responsible for some up-to-now unexplained phenomena observed in Si semiconductor research and device fabrication. Similar processing conditions for Si materials (namely, temperature and its variation in the presence of hydrogen and extended defects or interfaces) are often used in Si device manufacturing, which may lead to defect reactions that occur during the LeTID process.

Acknowledgements

The authors want to thank the partners from Fraunhofer IISB, ISC Konstanz, and the University of Konstanz for fabricating and characterizing solar cells and BMWK for funding the "ZORRO" project (contract no. 03EE1051D). Thanks are also due to Jan Beyer, Amy Albrecht, and Kuei-Shen Hsu (TU Bergakademie Freiberg) for their assistance with PL measurements and Steffanie Güldner (TU Bergakademie Freiberg) for help with sample preparations.

Open Access funding enabled and organized by Projekt DEAL.

Conflict of Interest

The authors declare no conflict of interest.

Author Contributions

Teimuraz Mchedlidze: conceptualization (lead); data curation (lead); formal analysis (lead); investigation (lead); methodology (lead); software (lead) supervision (equal); validation (lead); visualization (lead); writing—original draft (lead); writing—review & editing (equal). **Katharina Klose**: data curation (equal); investigation (supporting); methodology (supporting); visualization (supporting); writing—review & editing (supporting). **August Weber**: conceptualization (supporting); data curation (supporting); investigation (equal); methodology (equal); writing—review & editing (supporting). **Eugen Drubetskoi**: data curation (supporting); software (equal); visualization (supporting); writing—review & editing (supporting). **Johannes Heitmann**: conceptualization (equal); formal analysis (equal); project administration (equal); resources (equal); supervision (equal); writing—review & editing (equal). **Matthias Müller**: conceptualization (equal); data curation (equal); formal analysis (equal); funding acquisition (lead); investigation (equal); methodology (supporting); project administration (lead); resources (equal) software (equal); supervision (equal) writing—review & editing (equal).

Data Availability Statement

The data that support the findings of this study are available from the corresponding author upon reasonable request.

Keywords

defect-hydrogeninteraction in Si, Light- and elevated temperature-induced degradation, on-stage measurement method for PV cells, Si solar cell degradation

Received: February 20, 2025
Revised: March 21, 2025
Published online: April 3, 2025

[1] M. Bošnjaković, *Sustainability* **2024**, *16*, 7962.
[2] International Technology Roadmap for Photovoltaic (ITRPV)-vdma.org - VDMA, https://www.vdma.org/international-technology-roadmap-photovoltaic (accessed: March 2025).
[3] K. Ramspeck, S. Zimmermann, H. Nagel, A. Metz, Y. Gassenbauer, B. Birkmann, A. Seidl, in *27th Eur. Photovolt. Sol. Energy Conf. Exhib.*, Frankfurt, Germany September **2012**, pp. 861–865, https://doi.org/10.4229/27THEUPVSEC2012-2DO.3.4.
[4] F. Fertig, J. Broisch, D. Biro, S. Rein, *Sol. Energy Mater. Sol. Cells* **2014**, *121*, 157.
[5] F. Kersten, P. Engelhart, H.-C. Ploigt, A. Stekolnikov, T. Lindner, F. Stenzel, M. Bartzsch, A. Szpeth, K. Petter, J. Heitmann, J. W. Müller, *Sol. Energy Mater. Sol. Cells* **2015**, *142*, 83.

[6] D. Chen, P. G. Hamer, M. Kim, T. H. Fung, G. Bourret-Sicotte, S. Liu, C. E. Chan, A. Ciesla, R. Chen, M. D. Abbott, B. J. Hallam, S. R. Wenham, *Sol. Energy Mater. Sol. Cells* **2018**, *185*, 174.
[7] D. Chen, P. Hamer, M. Kim, C. Chan, A. Ciesla Nee Wenham, F. Rougieux, Y. Zhang, M. Abbott, B. Hallam, *Sol. Energy Mater. Sol. Cells* **2020**, *207*, 110353.
[8] D. Lin, Z. Hu, L. Song, D. Yang, X. Yu, *Sol. Energy* **2021**, *225*, 407.
[9] N. E. Grant, P. P. Altermatt, T. Niewelt, R. Post, W. Kwapil, M. C. Schubert, J. D. Murphy, *Sol. RRL* **2021**, *5*, 2000754.
[10] D. Chen, M. Vaqueiro Contreras, A. Ciesla, P. Hamer, B. Hallam, M. Abbott, C. Chan, *Prog. Photovoltaics* **2021**, *29*, 1180.
[11] L. Ning, L. Song, J. Zhang, *J. Alloys Compd.* **2022**, *912*, 165120.
[12] T. O. Abdul Fattah, V. P. Markevich, D. Gomes, J. Coutinho, N. V. Abrosimov, I. D. Hawkins, M. P. Halsall, A. R. Peaker, *Sol. Energy Mater. Sol. Cells* **2023**, *259*, 112447.
[13] J. Coutinho, D. Gomes, V. J. B. Torres, T. O. A. Fattah, V. P. Markevich, A. R. Peaker, *Sol. RRL* **2024**, *8*, 2300639.
[14] B. Hammann, P. Vieira Rodrigues, N. Aßmann, W. Kwapil, F. Schindler, M. C. Schubert, S. W. Glunz, *Sol. RRL* **2024**, *8*, 2400457.
[15] B. Hammann, F. Schindler, J. Schön, W. Kwapil, M. C. Schubert, S. W. Glunz, *Sol. Energy Mater. Sol. Cells* **2025**, *282*, 113432.
[16] A. Liu, S. P. Phang, D. Macdonald, *Sol. Energy Mater. Sol. Cells* **2022**, *234*, 111447.
[17] L. Song, Z. Hu, D. Lin, D. Yang, X. Yu, *J. Phys. Appl. Phys.* **2022**, *55*, 453002.
[18] M. Winter, D. C. Walter, J. Schmidt, *IEEE J. Photovoltaics* **2023**, *13*, 849.
[19] J. Simon, R. Fischer-Süßlin, R. Zerfaß, L. Kutschera, P. Dufke, A. Herguth, S. Roder, G. Hahn, *Sol. Energy Mater. Sol. Cells* **2023**, *260*, 112456.
[20] D. Bredemeier, D. Walter, S. Herlufsen, J. Schmidt, *AIP Adv.* **2016**, *6*, 035119.
[21] R. Eberle, W. Kwapil, F. Schindler, M. C. Schubert, S. W. Glunz, *Phys. Status Solidi RRL* **2016**, *10*, 861.
[22] K. Nakayashiki, J. Hofstetter, A. E. Morishige, T.-T. A. Li, D. B. Needleman, M. A. Jensen, T. Buonassisi, *IEEE J. Photovoltaics* **2016**, *6*, 860.
[23] C. E. Chan, D. N. R. Payne, B. J. Hallam, M. D. Abbott, T. H. Fung, A. M. Wenham, B. S. Tjahjono, S. R. Wenham, *IEEE J. Photovoltaics* **2016**, *6*, 1473.
[24] D. Bredemeier, D. C. Walter, J. Schmidt, *presented at the Siliconpv 2018, The 8th Int. Conf. on Crystalline Silicon Photovoltaics*, Lausanne, Switzerland March **2018**, p. 130001, https://doi.org/10.1063/1.5049320.
[25] T. Niewelt, F. Schindler, W. Kwapil, R. Eberle, J. Schön, M. C. Schubert, *Prog. Photovoltaics* **2018**, *26*, 533.
[26] T. Mchedlidze, M. M. Alam, A. Herguth, J. Weber, *Phys. Status Solidi A* **2019**, *216*, 1800918.
[27] T. Mchedlidze, J. Weber, *Phys. Status Solidi A* **2019**, *216*, 1900142.
[28] S. Johnston, C. Xiao, M. G. Deceglie, A. Gaulding, C.-S. Jiang, H. Guthrey, D. B. Kern, G. F. Kroeger, M. Al-Jassim, I. L. Repins, *IEEE J. Photovoltaics* **2022**, *12*, 703.
[29] D. Chen, M. Kim, B. V. Stefani, B. J. Hallam, M. D. Abbott, C. E. Chan, R. Chen, D. N. R. Payne, N. Nampalli, A. Ciesla, T. H. Fung, K. Kim, S. R. Wenham, *Sol. Energy Mater. Sol. Cells* **2017**, *172*, 293.
[30] A. Graf, A. Herguth, G. Hahn, in *presented at the AIP Conf. Proc., SiliconPV 2019, The 9th International Conference on Crystalline Silicon Photovoltaics*, Leuven, Belgium April **2019**, https://doi.org/10.1063/1.5123890.
[31] T. Mchedlidze, W. Seifert, M. Kittler, A. T. Blumenau, B. Birkmann, T. Mono, M. Müller, *J. Appl. Phys.* **2012**, *111*, 073504.
[32] T. Mchedlidze, K. Klose, A. Weber, E. Drubetskoi, M. Müller, J. Heitmann, in *GADEST 20/24, Gettering and Defect Engineering in Semiconductor Technology*, Bad Schandau, Germany, September **2024**, https://doi.org/10.13140/rg.2.2.17962.02243.
[33] T. Mchedlidze, Unpublished **2023**, https://doi.org/10.13140/RG.2.2.24131.78884.
[34] T. Mchedlidze, in *GADEST 20/24, Gettering and Defect Engineering in Semiconductor technology*, Bad Schandau, Germany, September **2024**, https://doi.org/10.13140/RG.2.2.13161.51044.
[35] M. S. Kim, J. H. Lee, M. K. Kwak, *Int. J. Precis. Eng. Manuf.* **2020**, *21*, 1389.
[36] T. Mchedlidze, L. Scheffler, J. Weber, M. Herms, J. Neusel, V. Osinniy, C. Möller, K. Lauer, *Appl. Phys. Lett.* **2013**, *103*, 013901.
[37] Z. Zhou, M. K. Juhl, M. Vaqueiro-Contreras, F. Rougieux, G. Coletti, *presented at the AIP Conf. Proc., SiliconPV 2021, The 11th International Conference on Crystalline Silicon Photovoltaics*, Hamelin, Germany, April **2022**, https://doi.org/10.1063/5.0089221.
[38] Z. Zhou, M. K. Juhl, M. Vaqueiro-Contreras, F. Rougieux, G. Coletti, *IEEE J. Photovoltaics* **2022**, *12*, 1369.
[39] J. T. Ryan, A. Matsuda, J. P. Campbell, K. P. Cheung, *Appl. Phys. Lett.* **2015**, *106*, 163503.
[40] M. K. Juhl, F. D. Heinz, G. Coletti, F. E. Rougieux, C. Sun, M. V. Contreras, T. Niewelt, J. Krich, M. C. Schubert, *IEEE J. Photovoltaics* **2023**, *13*, 524.
[41] M. Seibt, R. Khalil, V. Kveder, W. Schröter, *Appl. Phys. A* **2009**, *96*, 235.
[42] D. Cavalcoli, A. Cavallini, *Phys. Status Solidi C* **2007**, *4*, 2871.
[43] T. X. X. X. Mchedlidze, M. Kittler, *J. Appl. Phys.* **2012**, *111*, 053706.
[44] L. Wang, J. Liu, Y. Li, G. Wei, Q. Li, Z. Fan, H. Liu, Y. An, C. Liu, J. Li, Y. Fu, Q. Liu, D. He, *Adv. Energy Sustainability Res.* **2024**, *5*, 2300240.
[45] H. T. Nguyen, D. Yan, F. Wang, P. Zheng, Y. Han, D. Macdonald, *Phys. Status Solidi RRL* **2015**, *9*, 230.
[46] M. Tajima, T. Iwai, H. Toyota, S. Binetti, D. Macdonald, *J. Appl. Phys.* **2011**, *110*, 043506.
[47] H. Wu, H. T. Nguyen, A. Liu, D. Macdonald, *Prog. Photovoltaics* **2018**, *26*, 587.
[48] K. Peh, A. Flötotto, K. Lauer, D. Schulze, D. Bratek, S. Krischok, *Phys. Status Solidi B* **2023**, *260*, 2300300.
[49] R. R. Parsons, *Can. J. Phys.* **1978**, *56*, 814.
[50] J. Wagner, *Phys. Rev. B* **1984**, *29*, 2002.
[51] G. Davies, *Phys. Rep.* **1989**, *176*, 83.
[52] R. R. Parsons, *Solid State Commun.* **1979**, *29*, 763.
[53] V. V. Kveder, Y. A. Osipyan, I. R. Sagdeev, A. I. Shalynin, M. N. Zolotukhin, *Phys. Status Solidi A* **1985**, *87*, 657.
[54] J. I. Pankove, *Semiconductors and Semimetals*, Vol. *34*, Elsevier, Amsterdam, Netherlands **1991**, pp. 35–47, https://doi.org/10.1016/S0080-8784(08)62858-6.
[55] M. Matsubara, J. Godet, L. Pizzagalli, *J. Phys.: Condens. Matter* **2010**, *22*, 035803.
[56] C. Dubé, J. I. Hanoka, *Appl. Phys. Lett.* **1984**, *45*, 1135.
[57] W. M. R. Divigalpitiya, S. R. Morrison, G. Vercruysse, A. Praet, W. P. Gomes, *Sol. Energy Mater.* **1987**, *15*, 141.
[58] D. Cavalcoli, A. Cavallini, *Defects Diffus. Forum* **2005**, *245–246*, 15.
[59] M. Matsubara, J. Godet, L. Pizzagalli, *Phys. Rev. B* **2010**, *82*, 024107.
[60] C. P. Ewels, S. Leoni, M. I. Heggie, P. Jemmer, E. Hernández, R. Jones, P. R. Briddon, *Phys. Rev. Lett.* **2000**, *84*, 690.
[61] H. C. Sio, H. Wang, Q. Wang, C. Sun, W. Chen, H. Jin, D. Macdonald, *Sol. Energy Mater. Sol. Cells* **2018**, *182*, 98.
[62] D. Wu, T. Zhao, B. Ye, H. Chen, X. Liang, S. Li, D. Tian, D. Yang, X. Ma, *J. Appl. Phys.* **2023**, *134*, 155701.
[63] H. Li, K. Kim, B. Hallam, B. Hoex, S. Wenham, M. Abbott, *Front. Energy* **2017**, *11*, 42.
[64] J. S. Christensen, H. H. Radamson, A. Y. Kuznetsov, B. G. Svensson, *Appl. Phys. Lett.* **2003**, *82*, 2254.

[65] G. D. Watkins, *Mater. Sci. Semicond. Process.* **2000**, *3*, 227.
[66] C. A. Londos, E. N. Sgourou, D. Hall, A. Chroneos, *J. Mater. Sci.: Mater. Electron.* **2014**, *25*, 2395.
[67] V. V. Voronkov, R. Falster, *Mater. Sci. Eng., B* **2004**, *114–115*, 130.
[68] S. Agarwal, *Understanding the Mechanism of Light and Elevated Temperature Induced Degradation of P-Type Silicon Solar Cells (Final Report)*, Colorado School of Mines, Golden, CO **2023**, https://doi.org/10.2172/2008472.
[69] M. Wagner, F. Wolny, M. Hentsche, A. Krause, L. Sylla, F. Kropfgans, M. Ernst, R. Zierer, P. Bönisch, P. Müller, N. Schmidt, V. Osinniy, H.-P. Hartmann, R. Mehnert, H. Neuhaus, *Sol. Energy Mater. Sol. Cells* **2018**, *187*, 176.
[70] W. J. Taylor, T. Y. Tan, U. M. Gösele, *Appl. Phys. Lett.* **1991**, *59*, 2007.
[71] A. Borghesi, B. Pivac, A. Sassella, A. Stella, *J. Appl. Phys.* **1995**, *77*, 4169.
[72] D. Bredemeier, D. C. Walter, R. Heller, J. Schmidt, *Phys. Status Solidi RRL* **2019**, *13*, 1900201.
[73] T. Mchedlidze, M. Suezawa, *Phys. B: Condens. Matter* **2003**, *340–342*, 682.
[74] A. Nakanishi, N. Fukata, M. Suezawa, *Phys. Status Solidi B* **2003**, *235*, 115.
[75] M. Suezawa, *Phys. Rev. B* **2000**, *63*, 035203.
[76] M. Suezawa, *Phys. Rev. B* **2000**, *63*, 035201.
[77] A. J. Morris, C. J. Pickard, R. J. Needs, *Phys. Rev. B* **2008**, *78*, 184102.
[78] S. K. Estreicher, A. Docaj, M. B. Bebek, D. J. Backlund, M. Stavola, *Phys. Status Solidi A* **2012**, *209*, 1872.
[79] M. Suezawa, Y. Takada, T. Tamano, R. Taniguchi, F. Hori, R. Oshima, *Phys. Rev. B* **2002**, *66*, 155201.
[80] M. Budde, B. Bech Nielsen, P. Leary, J. Goss, R. Jones, P. R. Briddon, S. Öberg, S. J. Breuer, *Phys. Rev. B* **1998**, *57*, 4397.
[81] W. Düngen, R. Job, Y. Ma, Y. L. Huang, T. Mueller, W. R. Fahrner, L. O. Keller, J. T. Horstmann, H. Fiedler, *J. Appl. Phys.* **2006**, *100*, 034911.
[82] T. Mchedlidze, M. Suesawa, *Phys. Rev. B: Condens. Matter Mater. Phys.* **2004**, *70*, 205203-1.
[83] B. Hammann, N. Assmann, P. M. Weiser, W. Kwapil, T. Niewelt, F. Schindler, R. Sondena, E. V. Monakhov, M. C. Schubert, *IEEE J. Photovoltaics* **2023**, *13*, 224.
[84] E. Resmi, K. P. Sreejith, A. Kottantharayil, *Surf. Interfaces* **2023**, *38*, 102864.
[85] Y. Chibane, Y. Kouhlane, D. Bouhafs, W. Achour, A. Mohammed-Krarroubi, A. Khelfane, *Appl. Phys. A* **2024**, *130*, 367.
[86] M. U. Khan, D. Chen, S. Jafari, T. Ohshima, H. Abe, Z. Hameiri, C. M. Chong, M. Abbott, *Sol. Energy Mater. Sol. Cells* **2019**, *200*, 109990.
[87] T. H. Fung, M. Kim, D. Chen, C. E. Chan, B. J. Hallam, R. Chen, D. N. R. Payne, A. Ciesla, S. R. Wenham, M. D. Abbott, *Sol. Energy Mater. Sol. Cells* **2018**, *184*, 48.
[88] T. H. Fung, C. E. Chan, B. J. Hallam, D. N. R. Payne, M. D. Abbott, S. R. Wenham, *Energy Procedia* **2017**, *124*, 726.
[89] T. Luka, S. Großer, C. Hagendorf, K. Ramspeck, M. Turek, *Sol. Energy Mater. Sol. Cells* **2016**, *158*, 43.
[90] A. R. Meyer, P. C. Taylor, V. Lasalvia, X. Wang, W. Nemeth, M. Page, D. L. Young, S. Agarwal, P. Stradins, *Cell Rep. Phys. Sci.* **2023**, *4*, 101201.
[91] V. V. Kveder, Y. A. Osipyan, W. Schröter, G. Zoth, *Phys. Status Solidi A* **1982**, *72*, 701.
[92] V. A. Grazhulis, V. V. Kveder, Y. A. Osipyan, *Phys. Status Solidi B* **1981**, *103*, 519.
[93] M. Seibt, V. Kveder, W. Schröter, O. Voß, *Phys. Status Solidi A* **2005**, *202*, 911.
[94] J. Jablonski, B. Shen, T. Mchedlidze, M. Imai, K. Sumino, *Mater. Sci. Forum* **1995**, *196–201*, 1859.
[95] V. V. Voronkov, R. Falster, *J. Electrochem. Soc.* **2002**, *149*, G167.
[96] J. Vanhellemont, K. Nakamura, E. Kamiyama, K. Sueoka, *Defects and Impurities in Silicon Materials: An Introduction to Atomic-Level Silicon Engineering* (Eds: Y. Yoshida, G. Langouche), Springer Japan, Tokyo **2015**, pp. 181–240, https://doi.org/10.1007/978-4-431-55800-2_4.